NASA TECHNICAL NOTE

NASA TN D-5118

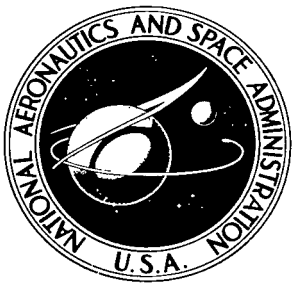

RESPONSE OF AN INFINITE ELASTIC PLATE TO AXISYMMETRIC INITIAL VELOCITY DISTRIBUTIONS WITH APPLICATION TO HYPERVELOCITY IMPACT

by Robert J. Hayduk

Langley Research Center
Langley Station, Hampton, Va.

NATIONAL AERONAUTICS AND SPACE ADMINISTRATION • WASHINGTON, D. C. • APRIL 1969

RESPONSE OF AN INFINITE ELASTIC PLATE TO AXISYMMETRIC INITIAL VELOCITY DISTRIBUTIONS WITH APPLICATION TO HYPERVELOCITY IMPACT

By Robert J. Hayduk

Langley Research Center
Langley Station, Hampton, Va.

NATIONAL AERONAUTICS AND SPACE ADMINISTRATION

For sale by the Clearinghouse for Federal Scientific and Technical Information
Springfield, Virginia 22151 – CFSTI price $3.00

RESPONSE OF AN INFINITE ELASTIC PLATE TO AXISYMMETRIC INITIAL VELOCITY DISTRIBUTIONS WITH APPLICATION TO HYPERVELOCITY IMPACT*

By Robert J. Hayduk
Langley Research Center

SUMMARY

Classical plate theory is used to study the response of an infinite plate to an axisymmetric initial velocity distribution over a central region. The expression for the bending stress is reduced to a single definite integral which depends upon the initial velocity distribution. The deflection is reduced to the Hankel inversion integral for three example distributions – conical, cylindrical, and spherical. The analysis indicates that the conical distribution causes larger stresses at the origin and deflections of the plate at short times after initiation than either the spherical or cylindrical distribution.

A simple relationship is derived for the failure thickness of an elastic plate responding to an axisymmetric initial momentum, monotonically decreasing in the radial direction. The failure-thickness relationship is shown to correlate with available experimental hypervelocity impact data where the initial momentum was induced by disk projectiles of various diameters.

INTRODUCTION

This paper presents a study of the response of an infinite, thin, elastic plate to an axisymmetric initial velocity distribution over a central region. The problem is directly related to an impulsively loaded plate, where the impulse is sufficiently distributed to ensure that the elastic plate action is the primary response and that the boundaries are

*Part of the information presented in this paper was included in a thesis entitled "The Response of a Single Wall Space Structure to Impact by Cometary Meteoroids of Various Shapes" which was submitted in partial fulfillment of the requirements for the degree of Master of Science in Engineering Mechanics, Virginia Polytechnic Institute, Blacksburg, Virginia, June 1968.

so remote that they do not influence the response until some time after the maximum stress occurs.

Classical plate theory, which neglects transverse shear and rotary inertia, has been used by many investigators to study the response of plates to impulsive loads. Reference 1 contains solutions to impulsively loaded infinite plate problems frequently referenced in the literature. Particular problems are an impulsive point force at the origin, an impulsive force uniformly distributed over a circular area, and an impulsive Gaussian distribution of pressure. In reference 2 the interaction of the spray from a meteoroid-penetrated bumper with the main wall of a double-walled structure was analyzed as a Gaussian distribution of initial momentum impacting on an infinite plate. Reference 3 showed that the deflections at a distance from the impact point of a large plate centrally impacted by a bullet agreed after a short time with those obtained by mathematically simulating the impact by an impulsive point force of finite duration on an infinite plate. Also presented in reference 3 are solutions to the impulsive point force problem for various time functions: finite duration, step function, and unit impulse function.

A large, highly concentrated impulse on a plate will cause plastic shear deformations. If, however, the impulse is distributed over a sufficiently large area, bending stresses will prevail, and the response of a plate can be well estimated by classical elastic plate theory. Axisymmetric distributed impulse loadings occur under certain circumstances on the second wall of a bumper-protected structure and on a single-wall structure impacted by cometary meteoroids of sufficiently low density. In the first case, the momentum of the spray from the pulverized bumper and meteoroid material imparts an initial velocity to the main wall; in the second case, the momentum of the low-density low-strength cometary meteoroid imparts an initial velocity to the single wall.

A general formula is derived for the maximum plate stress, and the response to three particular initial velocity distributions is examined in detail. A plate failure-thickness relationship is derived for an axisymmetric monotonically decreasing momentum impulse. Cometary meteoroid impact on a single-wall structure is considered as a momentum impulse and the form of the failure-thickness relationship is compared with available hypervelocity impact data.

SYMBOLS

a radius of central region given initial velocity

$A(p)$, $B(p)$ functions of p

$B(\alpha,\beta)$ beta function $\dfrac{\Gamma(\alpha)\Gamma(\beta)}{\Gamma(\alpha+\beta)}$ where α and β are the arguments

$c = \sqrt{\frac{E}{\rho}}$

d diameter

E modulus of elasticity

f geometric constant

${}_1F_1(\alpha;\beta;\xi)$, ${}_1F_2(\alpha;\beta;\gamma;\xi)$ hypergeometric functions where α,β,γ, and ξ are the arguments

h plate thickness

$i = \sqrt{-1}$

$J_0(p\eta)$ zeroeth-order Bessel function of first kind

$J_1(p\eta)$ first-order Bessel function of first kind

$J_{3/2}(p)$ fractional-order Bessel function of first kind

$k = \frac{2a^2}{ch}\sqrt{3(1 - \mu^2)}$

l length of projectile parallel to direction of motion

m mass

M magnitude of momentum per unit area at $\eta = 0$

n summation index

p Hankel transform parameter

Re( ) real part of complex variable

r radial coordinate

s Mellin transform parameter

ψ	shape factor
t	time
u,x	nondimensional variables of integration
$v(\eta)$	initial axisymmetric velocity distribution over a central region of radius a
$v'(\eta)$	dimensionless function specifying distribution of initial velocity or initial momentum
V	magnitude of initial velocity distribution (value at $\eta = 0$) or projectile velocity with subscript
$w(\eta,t)$	transverse displacement of midplane of plate
z	distance measured from and normal to midplane of plate
$\Gamma(\alpha)$, $\Gamma(\beta)$	gamma functions
∇^4	biharmonic operator
η	nondimensional radial coordinate, r/a
$\eta J_0(p\eta)$	kernel of Hankel transform
μ	Poisson's ratio
ρ	mass density (plate mass density without subscript)
σ	stress in general or stress at origin of plate

$$\tilde{\sigma}_p(\tau) = \frac{1}{4\tau}\int_0^1 uv'(u)\cos\left(\frac{u^2}{4\tau}\right)du$$

τ	nondimensional time, t/k

Subscripts:

co	conical
cr	critical
cyl	cylindrical
f	failure thickness
max	maximum
p	projectile
sph	spherical
$\theta\theta$	circumferential
$\eta\eta$	radial
ν	order

Superscripts:

λ,ν	constant exponents

A bar over a symbol denotes the Hankel transform; a tilde over a symbol denotes a nondimensional value. Dots over symbols denote differentiation with respect to time.

GOVERNING EQUATIONS

Definition of the Problem

Consider a thin, elastic plate infinite in extent with coordinates and dimensions as shown in figure 1. The plate's response to an initial axisymmetric velocity distribution $v(\eta)$ over a central region of radius a can be predicted by classical plate bending theory. The initial displacement of the plate is zero and the boundary and continuity conditions are prescribed by the transformed governing equation, that is, zero slope, finite curvature, and finite shear per unit length at the origin, and zero deflection, slope, curvature, and shear per unit length at infinity.

Transformed Governing Equation

The governing equation for the bending of a thin plate from linear, elastic, small-deflection theory is

$$\nabla^4 w = -k^2 \frac{\partial^2 w}{\partial t^2} \tag{1a}$$

where

$$k = \frac{2a^2}{ch}\sqrt{3(1 - \mu^2)} \tag{1b}$$

and the operator is

$$\nabla^4 = \left[\frac{1}{\eta}\frac{\partial}{\partial \eta}\left(\eta \frac{\partial}{\partial \eta}\right)\right]\left[\frac{1}{\eta}\frac{\partial}{\partial \eta}\left(\eta \frac{\partial}{\partial \eta}\right)\right] \tag{1c}$$

The deflection $w(\eta,t)$ is the transverse displacement of the midplane of the plate, a is the radius of the central region which is given the initial velocity distribution, $c = \sqrt{\frac{E}{\rho}}$, h is the plate thickness, μ is Poisson's ratio, and η is the nondimensional radial coordinate r/a.

Since the plate is infinite in extent, the problem is amenable to a zeroeth-order Hankel transform in the nondimensional radial coordinate η. The transform and its inverse are, respectively,

$$\bar{f}(p) = \int_0^\infty \eta f(\eta)\, J_0(p\eta)\, d\eta \tag{2a}$$

and

$$f(\eta) = \int_0^\infty p\bar{f}(p)\, J_0(p\eta)\, dp \tag{2b}$$

where p is the Hankel transform parameter and $\eta J_0(p\eta)$ is the kernel of the transform.

Application of the Hankel transform to the governing equation yields the following intermediate equation after integration by parts several times

$$\left\{\eta J_0(p\eta)\frac{\partial}{\partial \eta}\left[\frac{1}{\eta}\frac{\partial}{\partial \eta}\left(\eta \frac{\partial w}{\partial \eta}\right)\right] + p\frac{\partial}{\partial \eta}\left(\eta \frac{\partial w}{\partial \eta}\right) J_1(p\eta) - p^2\eta \frac{\partial w}{\partial \eta} J_0(p\eta) - p^3 w \eta J_1(p\eta)\right\}_{\eta=0}^{\infty} + k^2 \frac{d^2\bar{w}}{dt^2} + p^4\bar{w} = 0 \tag{3}$$

The term in braces vanishes at the upper and lower limit on η upon application of the appropriate boundary conditions at infinity and continuity conditions at the origin. At infinity, the deflection, slope, curvature, and shear per unit length are selected as zero and of the order necessary for the terms in braces to vanish. At the origin the continuity conditions are selected as zero slope, finite curvature, and finite shear per unit length. If the time is nondimensionalized to $\tau = \frac{t}{k}$, the transformed governing equation is

$$\frac{d^2\bar{w}}{d\tau^2} + p^4\bar{w} = 0 \tag{4}$$

GENERAL SOLUTION

The general solution to equation (4) is

$$\bar{w}(p,\tau) = A(p)\ \sin(p^2\tau) + B(p)\ \cos(p^2\tau) \tag{5}$$

where $A(p)$ and $B(p)$ are functions of the initial conditions on the plate. The function $B(p)$ is zero since the initial displacement, and hence the transformed initial displacement, is zero. The first derivative of equation (5) with respect to t relates $A(p)$ to the transformed initial velocity distribution; that is,

$$\dot{\bar{w}}(p,t) = \frac{1}{k}\frac{d\bar{w}(p,\tau)}{d\tau} \tag{6a}$$

$$\dot{\bar{w}}(p,t) = \frac{1}{k}\,p^2A(p)\ \cos(p^2\tau) \tag{6b}$$

Hence

$$A(p) = kp^{-2}\dot{\bar{w}}(p,0) \tag{7a}$$

$$A(p) = kp^{-2}\bar{v}(p) \tag{7b}$$

Substitution of equation (7b) into equation (5) with $B(p) = 0$ and application of the Hankel inversion integral (eq. (2b)) yields the displacement of the plate

$$w(\eta,\tau) = k\int_0^\infty p^{-1}\bar{v}(p)\ \sin(p^2\tau)J_0(p\eta)\ dp \tag{8}$$

Once the initial velocity distribution of particular interest is transformed, the displacement reduces to the inversion integral as shown by equation (8). The infinite integral usually defies analytical evaluation and must be evaluated numerically. Approximate methods for evaluating integral transforms and infinite integrals are available in standard mathematics references and usually exist as subroutines in computing programs.

With the displacement in inversion integral form, the stress, strain, shear, and moment distributions throughout the plate are easily obtained by differentiation and application of the same approximate methods for evaluating the integrals. Only loadings monotonically decreasing in the radial direction are considered in this paper. For such loadings the maximum stress, strain, and bending moment occur at the center. For these maximum responses the solution can be reduced to a single finite integral which is a function of the initial velocity distribution only.

Since $\left.\frac{\partial w}{\partial \eta}\right]_{\eta=0} = 0,$

$$\lim_{\eta \to 0} \frac{1}{\eta} \frac{\partial w}{\partial \eta} = \left.\frac{\partial^2 w}{\partial \eta^2}\right]_{\eta=0} \tag{9}$$

and the functional forms of the stress, strain, and bending moment at the origin are identical; therefore, the discussion in this paper is limited to the stress. From plate theory the normal radial and circumferential stresses at point z measured normal to the midplane are

$$\sigma_{\eta\eta} = - \frac{zE}{a^2(1 - \mu^2)} \left(\frac{\partial^2 w}{\partial \eta^2} + \frac{\mu}{\eta} \frac{\partial w}{\partial \eta} \right) \tag{10a}$$

and

$$\sigma_{\theta\theta} = - \frac{zE}{a^2(1 - \mu^2)} \left(\frac{1}{\eta} \frac{\partial w}{\partial \eta} + \mu \frac{\partial^2 w}{\partial \eta^2} \right) \tag{10b}$$

which, because of equation (9), reduce to

$$\sigma = \left.\sigma_{\eta\eta}\right]_{\eta=0} = \left.\sigma_{\theta\theta}\right]_{\eta=0} = \frac{-zE}{a^2(1 - \mu)} \left.\frac{\partial^2 w}{\partial \eta^2}\right]_{\eta=0} \tag{11}$$

Substitution of the transform integral (eq. (2a)) for $\bar{v}(p)$ into equation (8) yields

$$w(\eta, \tau) = k \int_0^1 uv(u) \int_0^\infty p^{-1} J_0(pu)\, J_0(p\eta)\, \sin(p^2\tau)\, dp\, du \tag{12}$$

if the order of integration is reversed. The upper limit on the first integral is unity because $v(\eta) = 0$ for $1 < \eta < \infty$. The second derivative of $w(\eta,\tau)$ with respect to η evaluated at $\eta = 0$ is

$$\left.\frac{\partial^2 w}{\partial \eta^2}\right]_{\eta=0} = -\frac{1}{2}k\int_0^1 uv(u)\int_0^\infty pJ_0(pu)\sin(p^2\tau)\,dp\,du$$

The infinite integral is evaluated in reference 1 as $\frac{1}{2\tau}\cos\left(\frac{u^2}{4\tau}\right)$ provided $\tau \neq 0$. The maximum stress occurs at the origin (eq. (11) with $z = h/2$) and is

$$\sigma(\tau) = \left(\frac{3(1+\mu)}{1-\mu}E\rho\right)^{1/2}\left[\frac{1}{4\tau}\int_0^1 uv(u)\cos\left(\frac{u^2}{4\tau}\right)du\right] \qquad (\tau \neq 0) \qquad (13)$$

Note that the maximum stress is a function of time. Thus the maximum stress (strain and bending moment resultant per unit length) at the origin has been reduced to a single finite integral which can be evaluated for any particular velocity distribution of interest.

SOLUTIONS FOR SPECIFIC VELOCITY DISTRIBUTIONS

In the following sections cylindrical, conical, and spherical initial velocity distributions are considered to demonstrate the application of equations (8) and (13). In the applications section the arbitrary magnitudes (V terms) of the example initial velocity distributions are related to a general axisymmetric momentum impulse monotonically decreasing in the radial direction.

Cylindrical Distribution

Consider the case where the central portion of the plate is given a uniform initial velocity; that is,

$$\left.\begin{aligned} v_{cyl}(\eta) &= V_{cyl} && (0 < \eta < 1) \\ v_{cyl}(\eta) &= 0 && (1 < \eta < \infty) \end{aligned}\right\} \qquad (14)$$

By application of equation (2a), $v_{cyl}(\eta)$ transforms as

$$\left.\begin{aligned} \bar{v}_{cyl}(p) &= V_{cyl}\int_0^1 \eta J_0(p\eta)\,d\eta \\ \bar{v}_{cyl}(p) &= V_{cyl}\,p^{-1}J_1(p) \end{aligned}\right\} \qquad (15)$$

Substitution of $\bar{v}_{cyl}(p)$ into equation (8) gives the displacement of the plate as

$$w_{cyl}(\eta,\tau) = kV_{cyl}\int_0^\infty p^{-2}J_1(p)\,J_0(p\eta)\,\sin(p^2\tau)\,dp \tag{16}$$

The maximum stress at the origin (eq. (13)) becomes

$$\sigma_{cyl}(\tau) = \left(\frac{3(1+\mu)}{1-\mu}\,E\rho\right)^{1/2}\frac{V_{cyl}}{4\tau}\int_0^1 u\cos\left(\frac{u^2}{4\tau}\right)du \qquad (\tau \neq 0) \tag{17a}$$

which readily integrates to

$$\sigma_{cyl}(\tau) = \frac{1}{2}\left(\frac{3(1+\mu)}{1-\mu}\,E\rho\right)^{1/2} V_{cyl}\,\sin(4\tau)^{-1} \qquad (\tau \neq 0) \tag{17b}$$

Conical Distribution

This distribution is expressed as a velocity linearly decreasing with radius; that is,

$$\left.\begin{aligned} v_{co}(\eta) &= V_{co}(1-\eta) && (0<\eta<1)\\ v_{co}(\eta) &= 0 && (1<\eta<\infty)\end{aligned}\right\} \tag{18}$$

Application of the transform to this $v(\eta)$ results in two integrals:

$$\bar{v}_{co}(p) = V_{co}\int_0^1 \eta\,J_0(p\eta)\,d\eta - V_{co}\int_0^1 \eta^2\,J_0(p\eta)\,d\eta \tag{19a}$$

The first integral is identical to equation (15); the second is evaluated in the appendix. For the conical distribution

$$\bar{v}_{co}(p) = V_{co}p^{-1}J_1(p) - \frac{1}{3}V_{co}\,{}_1F_2\left(\frac{3}{2};1,\frac{5}{2};-\frac{1}{4}p^2\right) \tag{19b}$$

The displacement becomes

$$w_{co}(\eta,\tau) = kV_{co}\int_0^\infty p^{-2}J_1(p)\,J_0(p\eta)\,\sin(p^2\tau)\,dp - \frac{1}{3}kV_{co}\int_0^\infty p^{-1}\,{}_1F_2\,J_0(p\eta)\,\sin(p^2\tau)\,dp \tag{20}$$

where the arguments of the hypergeometric function remain unchanged. Comparison of equations (20) and (16) indicates that the first integral represents the displacement due to

a uniform velocity distribution and the second integral represents the correction necessary to account for the linear decrease of velocity with radius.

For this case the maximum stress at the origin (eq. (13)) becomes

$$\sigma_{co}(\tau) = \left(\frac{3(1+\mu)}{1-\mu}\,E\rho\right)^{1/2} \frac{V_{co}}{4\tau}\int_0^1 u(1-u)\cos\left(\frac{u^2}{4\tau}\right)du \qquad (\tau \neq 0) \qquad (21a)$$

Integration by parts several times and a change of variables yields the Fresnel sine integral

$$\sigma_{co}(\tau) = \left(\frac{3(1+\mu)}{1-\mu}\,E\rho\right)^{1/2} V_{co}\tau^{1/2}\int_0^{(4\tau)^{-1/2}} \sin u^2\,du \qquad (21b)$$

For very small τ, approximate expressions exist for the integral to facilitate numerical integration.

Spherical Distribution

The distribution is given as

$$\left.\begin{aligned} v_{sph}(\eta) &= V_{sph}(1-\eta^2)^{1/2} \qquad (0<\eta<1)\\ v_{sph}(\eta) &= 0 \qquad\qquad\qquad\quad (1<\eta<\infty)\end{aligned}\right\} \qquad (22)$$

The transformed $v_{sph}(\eta)$ is

$$\bar{v}_{sph}(p) = V_{sph}\int_0^1 \eta(1-\eta^2)^{1/2}\,J_0(p\eta)\,d\eta \qquad (23a)$$

Evaluation of this integral (see appendix) yields

$$\bar{v}_{sph}(p) = V_{sph}\left(\frac{\pi}{2}\right)^{1/2} p^{-3/2}\,J_{3/2}(p) \qquad (23b)$$

The displacement for this example becomes

$$w_{sph}(\eta,\tau) = kV_{sph}\left(\frac{\pi}{2}\right)^{1/2}\int_0^\infty p^{-5/2}\,J_{3/2}(p)\,J_0(p\eta)\,\sin(p^2\tau)\,dp \qquad (24)$$

and the maximum stress at the origin

$$\sigma_{sph}(\tau) = \left(\frac{3(1+\mu)}{1-\mu}E\rho\right)^{1/2} \frac{V_{sph}}{4\tau}\int_0^1 u(1-u^2)^{1/2}\cos\left(\frac{u^2}{4\tau}\right)du \qquad (\tau \neq 0) \qquad (25a)$$

The integral is evaluated in the appendix and yields

$$\sigma_{sph}(\tau) = \frac{\pi^{1/2}}{4}\left(\frac{3(1+\mu)}{1-\mu}E\rho\right)^{1/2} V_{sph}\sum_{n=0}^{\infty}\frac{(-1)^n(4\tau)^{-(2n+1)}}{\Gamma\left(2n+\frac{5}{2}\right)} \qquad (\tau \neq 0) \qquad (25b)$$

For very small τ, an asymptotic expansion for the series facilitates convergence.

RESULTS AND DISCUSSION

As a basis for comparing the effects of the three example distributions, the velocity magnitudes (V terms) were selected to give the plates the same total initial momentum. This basis was chosen to facilitate application to a general axisymmetric initial momentum impulse monotonically decreasing in the radial direction.

If the diameters of the central regions and the total initial momentums are equal in all three cases, the velocity magnitudes are related. The total initial momentums for the three cases are:

$$\text{Momentum}_{cyl} = \pi a^2 h\rho V_{cyl} \qquad (26a)$$

$$\text{Momentum}_{co} = \frac{1}{3}\pi a^2 h\rho V_{co} \qquad (26b)$$

$$\text{Momentum}_{sph} = \frac{2}{3}\pi a^2 h\rho V_{sph} \qquad (26c)$$

The second and third momentum expressions equal the first if

$$V_{co} = 3V_{cyl} \qquad (26d)$$

$$V_{sph} = \frac{3}{2}V_{cyl} \qquad (26e)$$

To demonstrate the effect that the shape of the initial velocity distribution has on the displacement of the plate, the deflection at $\tau = 0.15$, 0.4, 0.6, and 1.0 (eqs. (16), (20), and (24)) is presented in figure 2 for the equivalent magnitudes of V_{cyl}, $3V_{cyl}$, and $\frac{3}{2}V_{cyl}$ for the cylindrical, conical, and spherical distributions, respectively. The

ordinate in the plots is the nondimensional displacement obtained by dividing the actual displacement by kV_{cyl}.

Figure 2 indicates that the conical initial velocity distribution causes the largest displacement of the plate at a particular time and the cylindrical distribution, the least. The differences in deflection caused by the various velocity distributions are large initially, and then diminish with time. By $\tau = 1.0$, the deflection of the plate is nearly the same for all three distributions.

The maximum bending stress at the origin of the plate for the three example velocity distributions (eqs. (17b), (21b), and (25b)) with the magnitudes given by equation (26) is presented in figure 3 for τ ranging from 0 to 0.7. The ordinate parameter is the nondimensional stress $\left(\frac{1 - \mu}{3(1 + \mu)E\rho}\right)^{1/2} \frac{\sigma(\tau)}{V_{cyl}}$. In all three cases a distinct peak occurs and then the stresses rapidly converge. The peak stresses for the conical and spherical distributions are 1.58 and 1.22 times that of the cylindrical distribution. Hence, the peak stress at the origin also indicates that the conical initial velocity distribution causes larger responses of the plate than either the spherical or cylindrical distributions. Since it is known that classical plate theory predicts a spurious response at all points of the plate immediately after application of a sharp impulse (ref. 3), the irregular stress variations occurring between τ equal to 0 and 0.1 are thought to be mathematical anomalies rather than physical phenomena.

The results for the displacement and stress at the origin for the three equivalent velocity distributions indicate, as one would expect, that a plate resists a more distributed impulse load better than a concentrated one.

APPLICATIONS

General Momentum Impulse

Frequently in design, the minimum plate thickness to prevent failure due to an impulse is required. Such a design equation can be obtained from the preceding analysis for a general, axisymmetric, monotonically decreasing momentum impulse on an infinite plate.

If $Mv'(\eta)$ is the momentum per unit area imparted to the central portion of radius a of an infinite plate where M is the magnitude at $\eta = 0$ and $v'(\eta)$ is a dimensionless function specifying the distribution, the initial velocity of the plate is

$$\left.\begin{aligned} v(\eta) &= \frac{M}{\rho h} v'(\eta) \qquad (0 < \eta < 1) \\ v(\eta) &= 0 \qquad\qquad\quad (1 < \eta < \infty) \end{aligned}\right\} \tag{27}$$

Substitution of $\frac{M}{\rho h} v'(\eta)$ for $v(\eta)$ in equation (13) gives

$$\sigma(\tau) = \left(\frac{3(1+\mu)}{1-\mu}\frac{E}{\rho}\right)^{1/2} \frac{M}{h}\frac{1}{4\tau}\int_0^1 uv'(u)\cos\left(\frac{u^2}{4\tau}\right) du \tag{28}$$

The $M/\rho h$ factors are specific values of V_{cyl}, V_{co}, and V_{sph} of the previous example velocity distributions for cylindrical, conical, and spherical momentum distributions, respectively. The thickness of the plate which will just resist failure is of main interest. If one assumes that the response of the plate is bending and elastic until failure, the maximum stress at failure will be some critical stress σ_{cr} and the plate failure thickness some h_f. Let $\left(\tilde{\sigma}_p\right)_{max}$ be the maximum value of $\tilde{\sigma}_p$ where

$$\tilde{\sigma}_p = \frac{1}{4\tau}\int_0^1 uv'(u)\cos\left(\frac{u^2}{4\tau}\right) du$$

Equation (28) then becomes

$$\sigma_{cr} = \left(\frac{3(1+\mu)}{1-\mu}\frac{E}{\rho}\right)^{1/2} \frac{M}{h_f}\left(\tilde{\sigma}_p\right)_{max} \tag{29}$$

or when solved for the failure thickness,

$$h_f = \frac{\left(\tilde{\sigma}_p\right)_{max}}{\sigma_{cr}}\left(\frac{3(1+\mu)}{1-\mu}\frac{E}{\rho}\right)^{1/2} M \tag{30}$$

Hypervelocity Impact

Spacecraft designers need design equations to specify the thickness of both single- and double-walled space vehicles to prevent penetration by particulate debris (meteoroids) while in space. Equation (30) can be applied to the impact of a cometary meteoroid with a single-walled space structure and to the impact of the spray emanated from the bumper with the main wall of a double-walled structure. However, the discussion here will be restricted to cometary meteoroid impact on single-walled space structures since the momentum per unit area distribution of the meteoroid-bumper spray cannot be defined at this time in terms of bumper and meteoroid parameters.

The assumptions made about the phenomena are: momentum exchange is the primary mechanism of interaction; the time of exchange is instantaneous; and the momentum of the impacting mass is negligible with respect to the momentum of the wall after impact.

For axisymmetric cometary meteoroids,

$$M = \rho_p l_p V_p \tag{31}$$

where ρ_p, l_p, and V_p are the meteoroid density, length, and velocity, respectively. For the simple axisymmetric examples considered here the meteoroid mass density ρ_p can be expressed as

$$\rho_p = \frac{f_p m_p}{\pi d^2 l_p} \tag{32}$$

where f_p is a geometric constant. For cylinders, cones, and spheres, f_p has values of 4, 12, and 6, respectively. Equations (31) and (32) substituted into equation (30) yield

$$h_f = \psi \frac{1}{\sigma_{cr}} \left(\frac{3(1 + \mu)}{1 - \mu} \frac{E}{\rho} \right)^{1/2} \frac{m_p V_p}{d^2} \tag{33}$$

where $\psi = \dfrac{f_p \left(\tilde{\sigma}_p\right)_{max}}{\pi}$ is a factor depending only on the shape of the meteoroids.

Low-density projectiles are difficult to launch in the laboratory; consequently, there are no single-wall data available which simulate the conditions assumed in this analysis. However, data are reported in reference 4 where plastic film disks (ref. 5) of different diameters impacted aluminum plates. The failure thicknesses for both projectiles were shown to vary as projectile velocity to the first power. However, if the data are plotted as failure thickness h_f, as a function of total projectile momentum per unit area $\dfrac{m_p V_p}{d^2}$, as in figure 4, this relationship is also approximately linear.

Values of $\left(\tilde{\sigma}_p\right)_{max}$ can be obtained from figure 3 by noting that the curves actually plotted in the three cases are $3\tilde{\sigma}_{co}(\tau)$, $\frac{3}{2}\tilde{\sigma}_{sph}(\tau)$, and $\tilde{\sigma}_{cyl}(\tau)$. The curves were plotted in this manner to give the plates the same total initial momentum. One needs only to estimate the peak values in the figure and multiply by 1/3 and 2/3, respectively, to arrive at $\left(\tilde{\sigma}_{co}\right)_{max} = 0.264$, $\left(\tilde{\sigma}_{sph}\right)_{max} = 0.408$, and $\left(\tilde{\sigma}_{cyl}\right)_{max} = \frac{1}{2}$. Substitution of these values of $\left(\tilde{\sigma}_p\right)_{max}$ along with the appropriate values of f_p into the shape factors yields

$$\psi_{cyl} = \frac{2}{\pi} \tag{34a}$$

$$\psi_{co} = \frac{3.17}{\pi} \tag{34b}$$

$$\psi_{sph} = \frac{2.45}{\pi} \tag{34c}$$

Thus equations (33) and (34) indicate that a single-walled structure of a space vehicle must be made thicker to prevent failure due to impact by a conical meteoroid than by either a spherical or cylindrical meteoroid when all three have the same momentum and diameter at impact.

Richard Madden, Langley Research Center, 1967, employing similar methods, obtained an identical expression (unpublished) for equations (33) and (34a) for the particular problem of a right circular cylinder.

CONCLUDING REMARKS

Linear, elastic, small-deflection plate theory was used to study the response of an infinite plate to an axisymmetric initial velocity distribution over a central region. The stress at the origin was reduced to a single definite integral which depends upon only the initial velocity distribution and the deflection was reduced to a Hankel inversion integral for three example distributions.

Cylindrical, conical, and spherical initial velocity distributions, which gave the plate the same total initial momentum, were studied to demonstrate the application of the equations and to compare the effects of varying the distribution. The analysis indicated that the conical distribution caused larger deflections and stresses in the plate than either the spherical or cylindrical distribution.

A simple relationship was derived for the failure thickness of an elastic plate responding to an axisymmetric initial momentum, monotonically decreasing in the radial direction. The failure-thickness relationship was shown to correlate with available experimental hypervelocity impact data where the initial momentum was induced by disk projectiles of various diameters.

Langley Research Center,
National Aeronautics and Space Administration,
Langley Station, Hampton, Va., February 4, 1969,
124-08-01-21-23.

APPENDIX

EVALUATION OF INTEGRALS

Three integrals which appear in the text are evaluated in this appendix. The three integrals are evaluated by considering them to be Mellin transforms of particular functions and by selecting the appropriate value for the transform parameter.

By definition the Mellin transform of a function is

$$g(s) = \int_0^\infty f(u)u^{s-1}\,du \tag{A1}$$

The integral

$$\int_0^1 \eta^2 J_0(p\eta)\,d\eta$$

which appears in equation (19a) can be considered as the Mellin transform of

$$\left.\begin{aligned} f(\eta) &= J_\nu(p\eta) \qquad (0 < \eta < 1) \\ f(\eta) &= 0 \qquad\quad (1 < \eta < \infty) \end{aligned}\right\} \tag{A2}$$

with ν equal to zero and s equal to 3. The transform of equation (A2) is given in reference 6 (p. 326) as

$$\frac{p^\nu}{2^\nu(s+\nu)\Gamma(\nu+1)}\,{}_1F_2\left(\frac{s+\nu}{2};\nu+1,\frac{s+\nu}{2}+1;-\frac{1}{4}p^2\right) \tag{A3}$$

which yields

$$\int_0^1 \eta^2 J_0(p\eta)\,d\eta = \frac{1}{3}\,{}_1F_2\left(\frac{3}{2};1,\frac{5}{2};-\frac{1}{4}p^2\right) \tag{A4}$$

The integral

$$\int_0^1 \eta(1-\eta^2)^{1/2} J_0(p\eta)d\eta \tag{A5}$$

which appears in equation (23a) can also be evaluated as a Mellin transform. On page 327 of reference 6 the Mellin transform of

APPENDIX

$$\left.\begin{aligned} f(\eta) &= (1 - \eta^2)^{\lambda} J_{\nu}(p\eta) \qquad (0 < \eta < 1) \\ f(\eta) &= 0 \qquad\qquad\qquad\quad (1 < \eta < \infty) \end{aligned}\right\} \tag{A6}$$

is given as

$$\frac{p^{\nu} B\left(\lambda + 1, \frac{1}{2}s + \frac{1}{2}\nu\right)}{2^{\nu+1}\,\Gamma(\nu + 1)}\, {}_1F_2\left(\frac{s + \nu}{2}; \nu + 1, \frac{s + \nu}{2} + 1 + \lambda; -\frac{1}{4}p^2\right) \tag{A7}$$

provided $\mathrm{Re}\ \lambda > -1$ and $\mathrm{Re}\ s > -\mathrm{Re}\ \nu$. With $\nu = 0$, $s = 2$, and $\lambda = \frac{1}{2}$, equation (A5) is evaluated as

$$\int_0^1 \eta(1 - \eta^2)^{1/2} J_0(p\eta)\, d\eta = \frac{1}{3}\, {}_1F_2\left(1; 1, \frac{5}{2}; -\frac{1}{4}p^2\right) \tag{A8}$$

The identical numerator and denominator parameters of the hypergeometric function cancel and leave ${}_0F_1\left(\frac{5}{2}; -\frac{1}{4}p^2\right)$. This hypergeometric function is related to the Bessel functions by the relationship (ref. 7, p. 100)

$$J_{\nu}(p) = \frac{\left(\frac{1}{2}p\right)^{\nu}}{\Gamma(\nu + 1)}\, {}_0F_1\left(\nu + 1; -\frac{1}{4}p^2\right) \tag{A9}$$

By use of this relationship, the hypergeometric function can be expressed as

$${}_0F_1\left(\frac{5}{2}; -\frac{1}{4}p^2\right) = 3\left(\frac{\pi}{2}\right)^{1/2} p^{-3/2} J_{3/2}(p) \tag{A10}$$

and the final result as

$$\int_0^1 \eta(1 - \eta^2)^{1/2} J_0(p\eta)\, d\eta = \left(\frac{\pi}{2}\right)^{1/2} p^{-3/2} J_{3/2}(p) \tag{A11}$$

The integral

$$\frac{1}{4\tau}\int_0^1 \eta(1 - \eta^2)^{1/2} \cos\left(\frac{\eta^2}{4\tau}\right) d\eta \tag{A12}$$

which appears in equation (25a) requires a simple change of variables to convert it to a Mellin transform. Let $x = \eta^2$ and $b = \frac{1}{4\tau}$; then the integral becomes

APPENDIX

$$\frac{1}{8\tau}\int_0^1 (1 - x)^{1/2} \cos(bx)\, dx \tag{A13}$$

On page 320 of reference 6, the Mellin transform of

$$\left.\begin{aligned} f(x) &= (1 - x)^{\nu-1}\cos(bx) \qquad (0 < x < 1;\ \mathrm{Re}\ \nu > 0) \\ f(x) &= 0 \qquad\qquad\qquad\quad (1 < x < \infty;\ \mathrm{Re}\ \nu > 0) \end{aligned}\right\} \tag{A14}$$

is given as

$$\frac{1}{2} B(s,\nu)\left[{}_1F_1(s;s + \nu;ib) + {}_1F_1(s;s + \nu;-ib)\right] \tag{A15}$$

for $\mathrm{Re}\ s > 0$. By letting ν be 3/2 and s be 1, the desired integral becomes

$$\int_0^1 (1 - x)^{1/2}\cos(bx)\, dx = \frac{1}{3}\left[{}_1F_1\left(1;\frac{5}{2};ib\right) + {}_1F_1\left(1;\frac{5}{2};-ib\right)\right] \tag{A16}$$

The confluent hypergeometric function is the power series

$$\left.\begin{aligned} {}_1F_1(\alpha;\beta;\xi) &= 1 + \frac{\alpha}{\beta}\frac{\xi}{1!} + \frac{\alpha(\alpha+1)}{\beta(\beta+1)}\frac{\xi^2}{2!} + \cdots \\ {}_1F_1(\alpha;\beta;\xi) &= \sum_{n=0}^{\infty} \frac{(\alpha)_n}{(\beta)_n}\frac{\xi^n}{n!} \end{aligned}\right\} \tag{A17}$$

where Pochhammer's notation used for the numerator and denominator parameters is

$$(\alpha)_n = \alpha(\alpha + 1)(\alpha + 2) \cdots (\alpha + n - 1) \tag{A18}$$

and

$$(\alpha)_0 = 1$$

Adding the confluent hypergeometric functions of equation (A16) term by term eliminates all the imaginary terms. In general, then

$${}_1F_1(\alpha;\beta;i\xi) + {}_1F_1(\alpha;\beta;-i\xi) = 2\sum_{n=0}^{\infty} (-1)^n \frac{(\alpha)_{2n}\xi^{2n}}{(\beta)_{2n}(2n)!} \tag{A19}$$

These results give

$$\frac{1}{4\tau}\int_0^1 \eta(1-\eta^2)^{1/2}\cos\left(\frac{\eta^2}{4\tau}\right)d\eta = \frac{1}{12\tau}\sum_{n=0}^{\infty}(-1)^n\frac{(1)_{2n}(4\tau)^{-2n}}{\left(\frac{5}{2}\right)_{2n}(2n)!} \tag{A20}$$

which reduces to

$$\frac{1}{4\tau}\int_0^1 \eta(1-\eta^2)^{1/2}\cos\left(\frac{\eta^2}{4\tau}\right)d\eta = \frac{\pi^{1/2}}{4}\sum_{n=0}^{\infty}\frac{(-1)^n(4\tau)^{-(2n+1)}}{\Gamma\left(2n+\frac{5}{2}\right)} \tag{A21}$$

An asymptotic expansion of the series for very small τ is easily obtainable by adding the asymptotic expansions of the two confluent hypergeometric functions in equation (A19).

REFERENCES

1. Sneddon, Ian N.: Fourier Transforms. First ed., McGraw-Hill Book Co., Inc., 1951.

2. Madden, Richard: Ballistic Limit of Double-Walled Meteoroid Bumper Systems. NASA TN D-3916, 1967.

3. Medick, M. A.: On Classical Plate Theory and Wave Propagation. Trans. ASME, Ser. E.: J. Appl. Mech., vol. 28, no. 2, June 1961, pp. 223-228.

4. Alfaro-Bou, Emilio; and Thomson, Robert G.: Ballistic Limit of Aluminum Plates Determined by an Exploding Foil Gun Technique. NASA TN D-4259, 1967.

5. Mylar – Physical, Electrical, and Chemical Properties. Tech. Rep. TR-1, E. I. Du Pont de Nemours & Co., Inc.

6. Staff of the Bateman Manuscript Project, compiler: Tables of Integral Transforms. Vol. I. McGraw-Hill Book Co., Inc., 1954.

7. Watson, G. N.: A Treatise on the Theory of Bessel Functions. Second ed., The Macmillan Co., 1944.

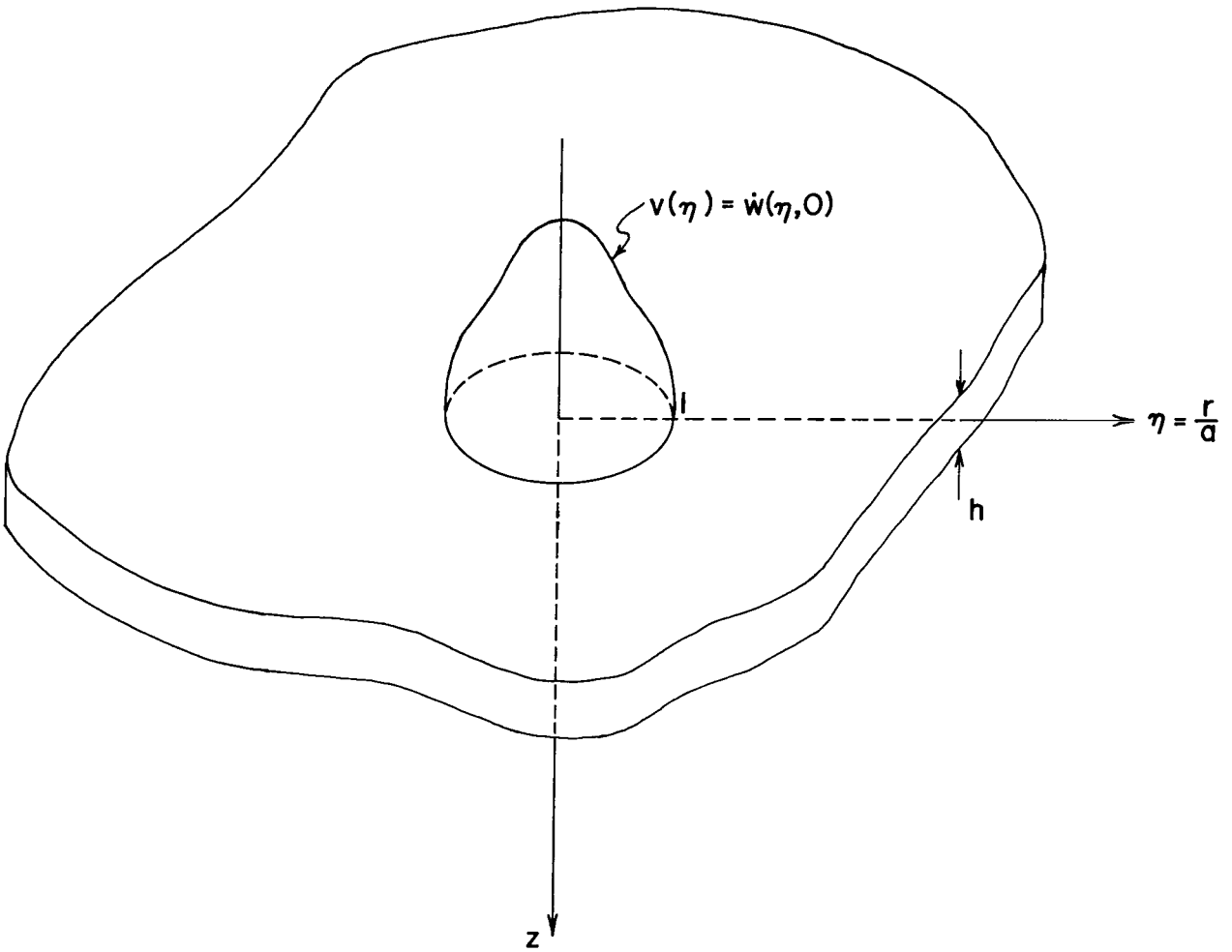

Figure 1.- Configuration of thin, elastic plate infinite in extent with initial velocity distribution.

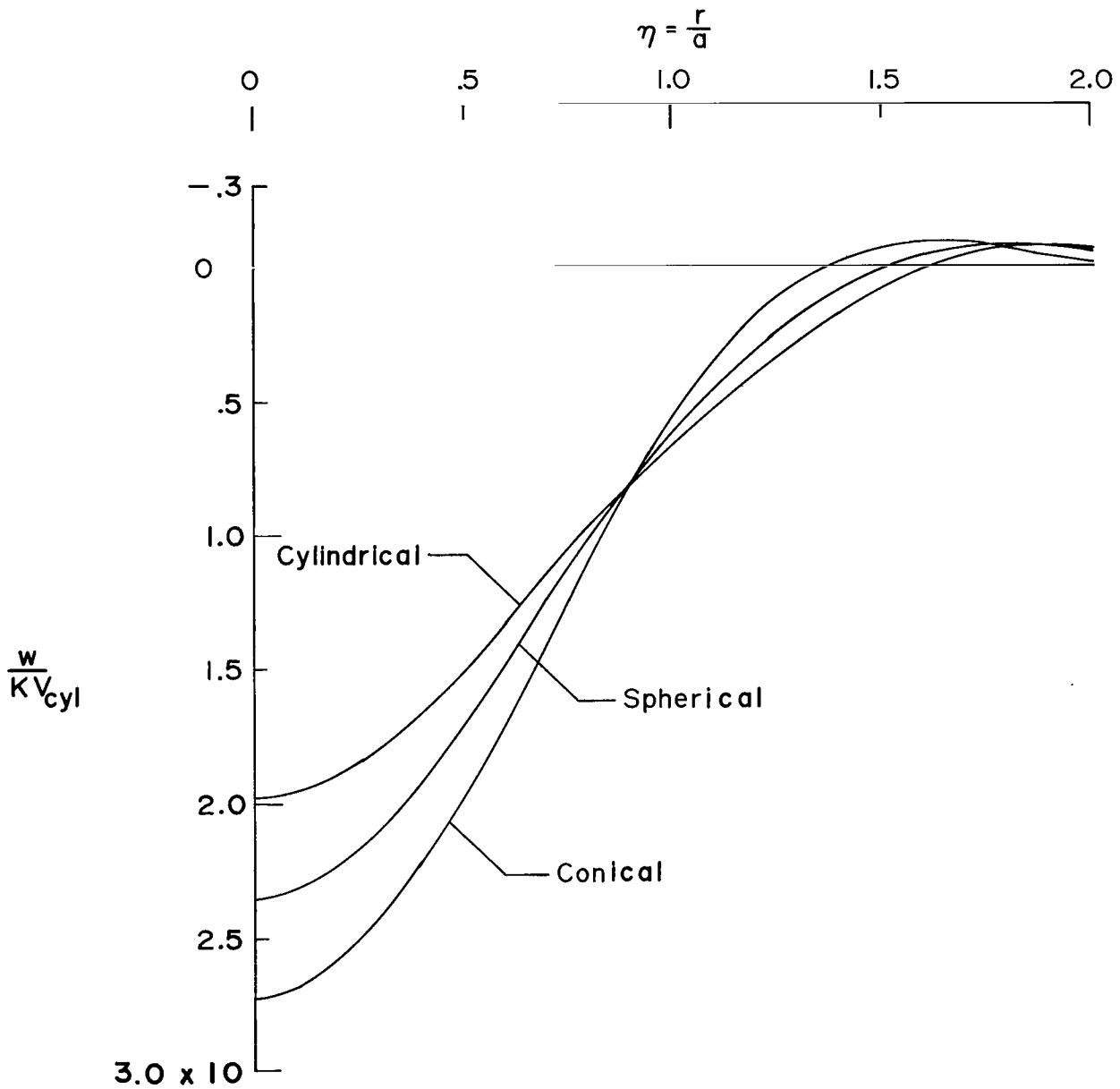

(a) $\tau = 0.15$.

Figure 2.- Comparison of the plate's deflection at various nondimensional times for the three initial velocity distributions.

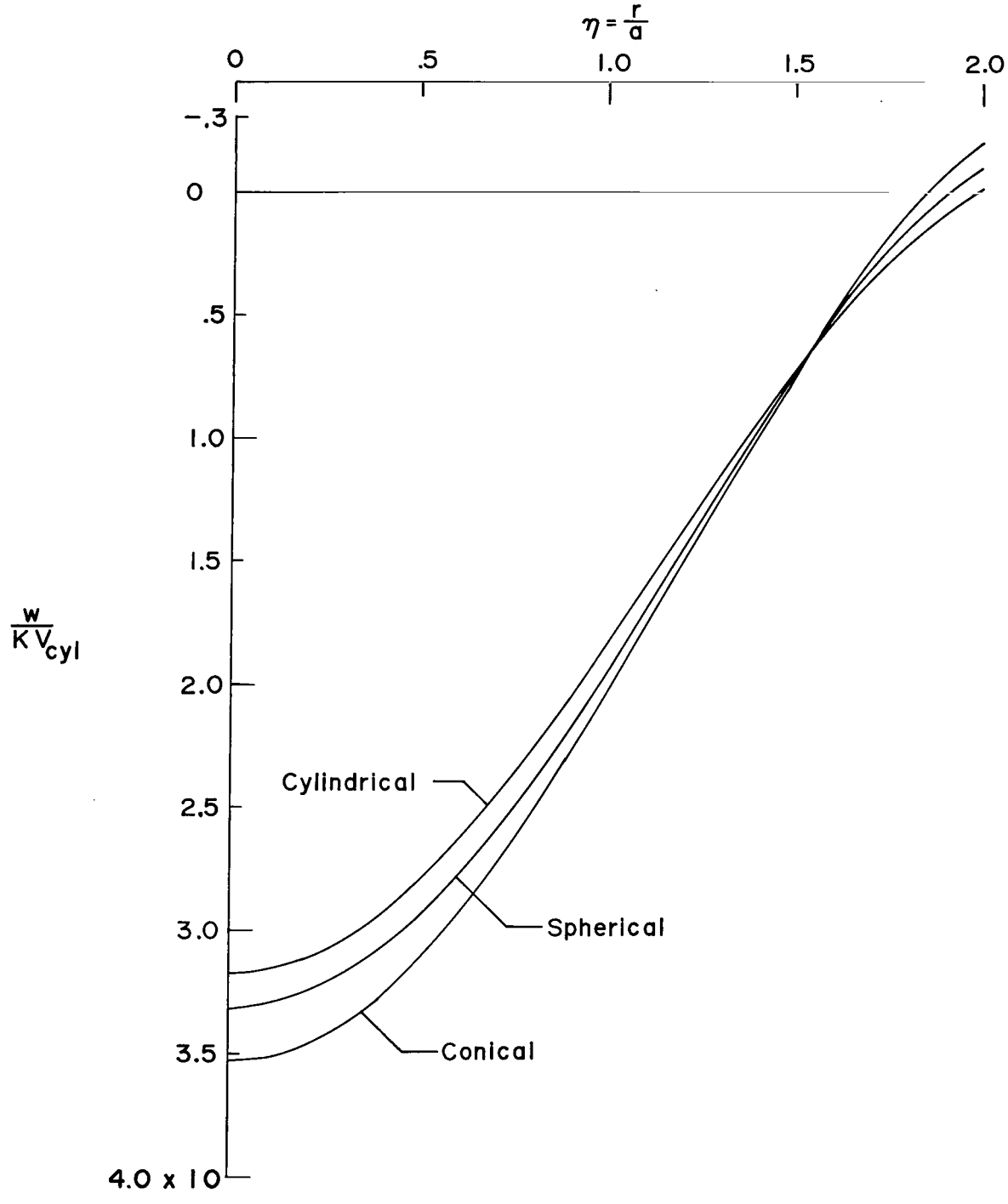

(b) $\tau = 0.4$.

Figure 2.- Continued.

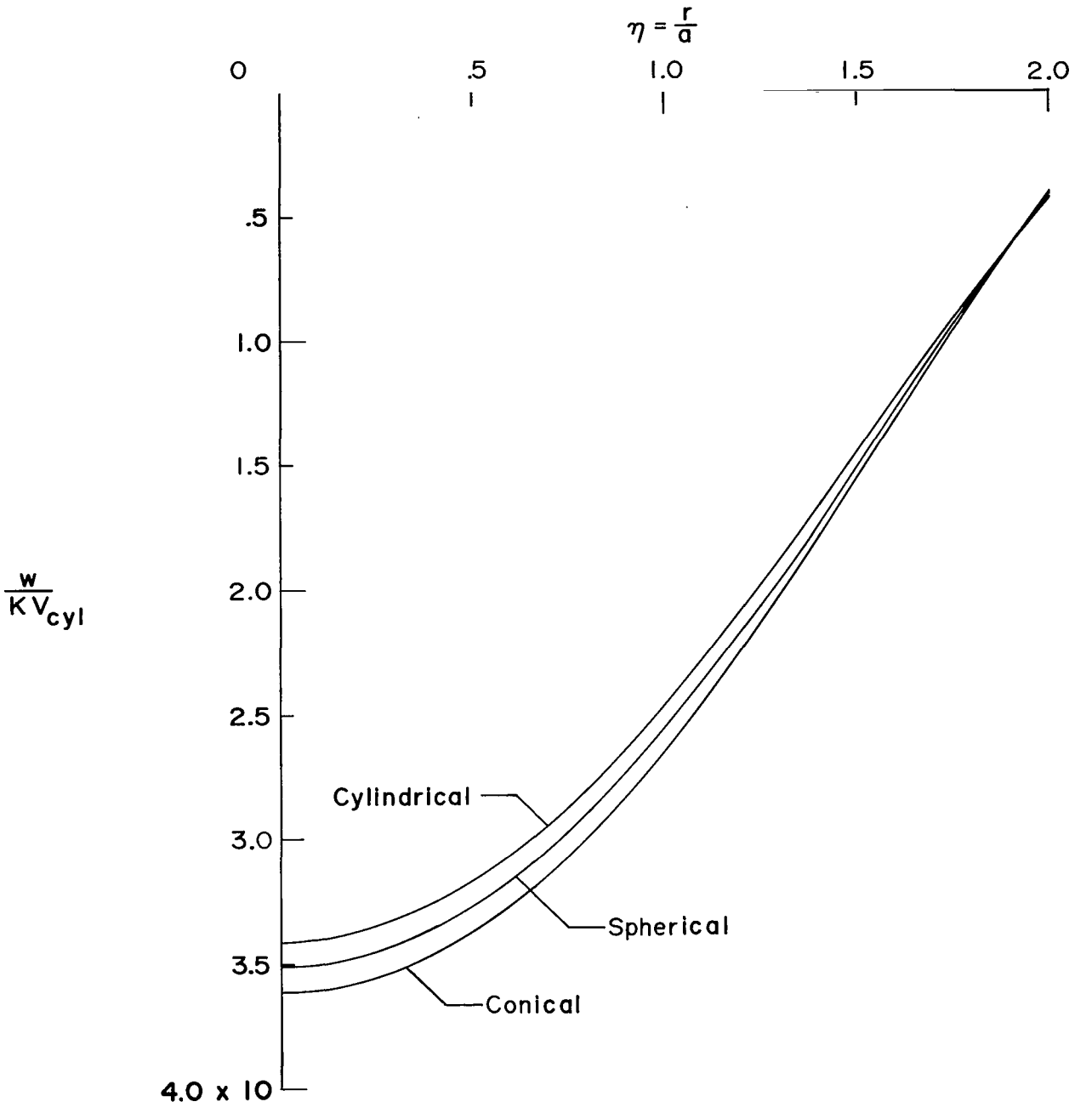

(c) $\tau = 0.6$.

Figure 2.- Continued.

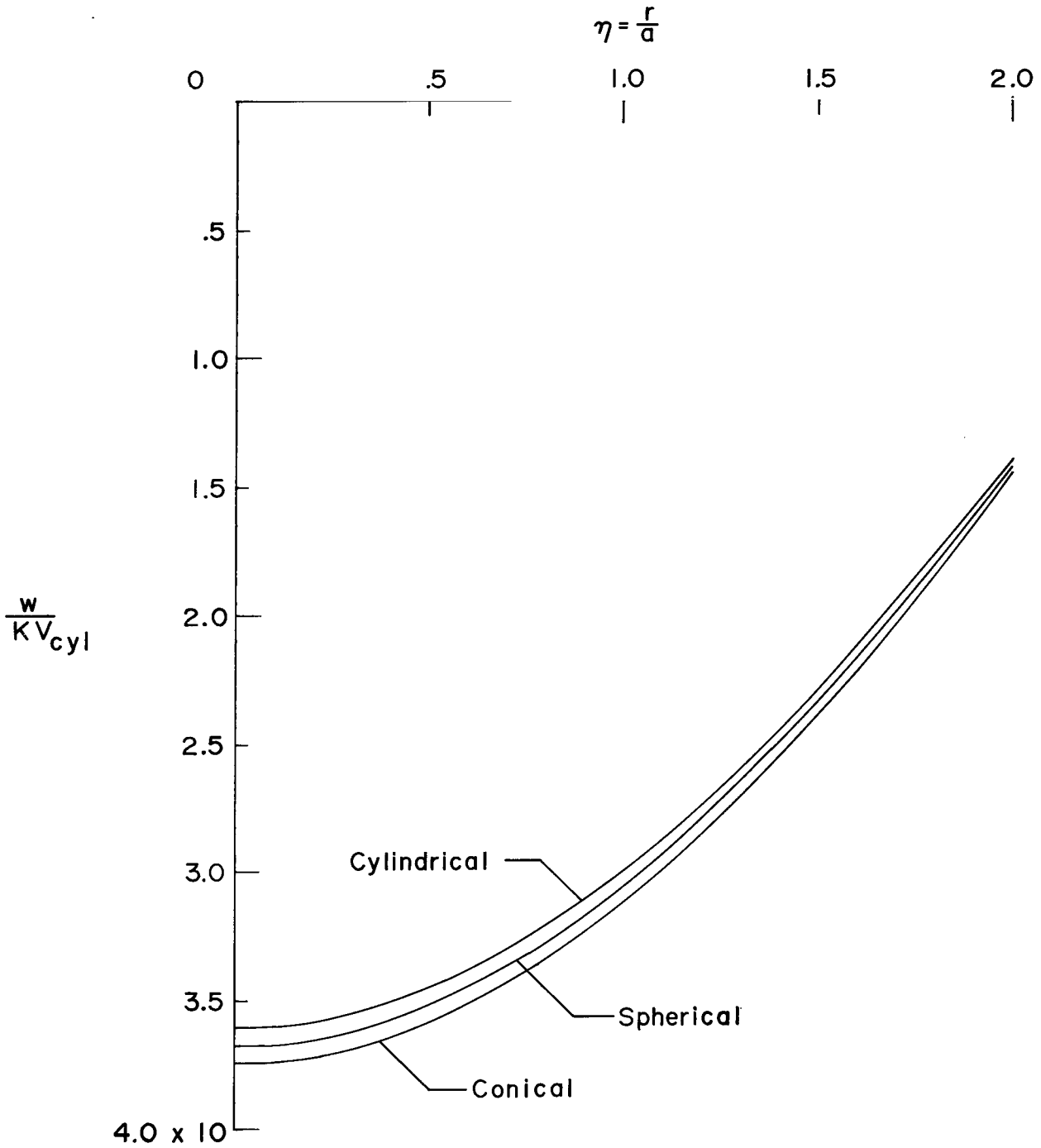

(d) τ = 1.0.

Figure 2.- Concluded.

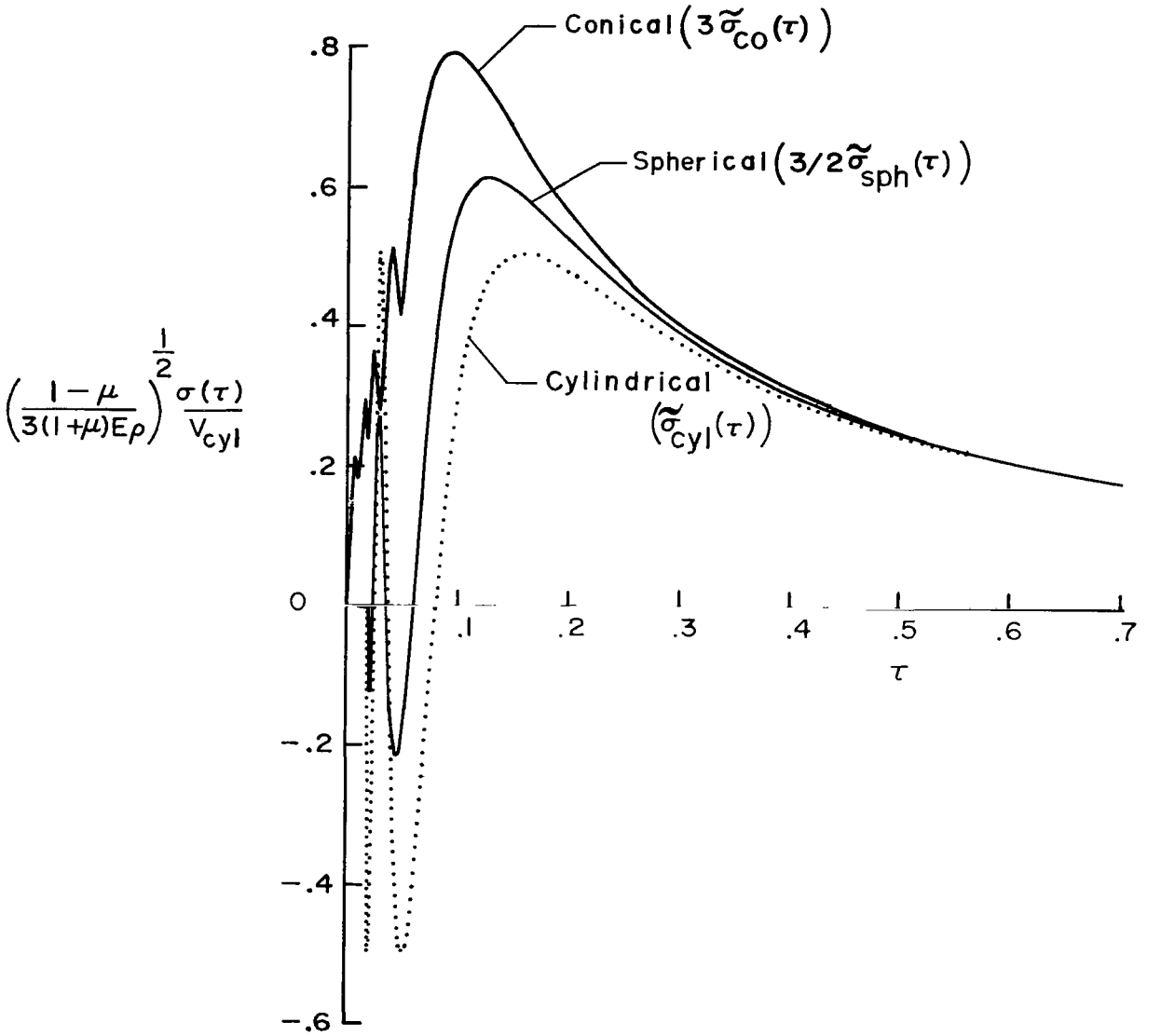

Figure 3.- Variation of the maximum stress at the origin with time for the three example initial velocity distributions.

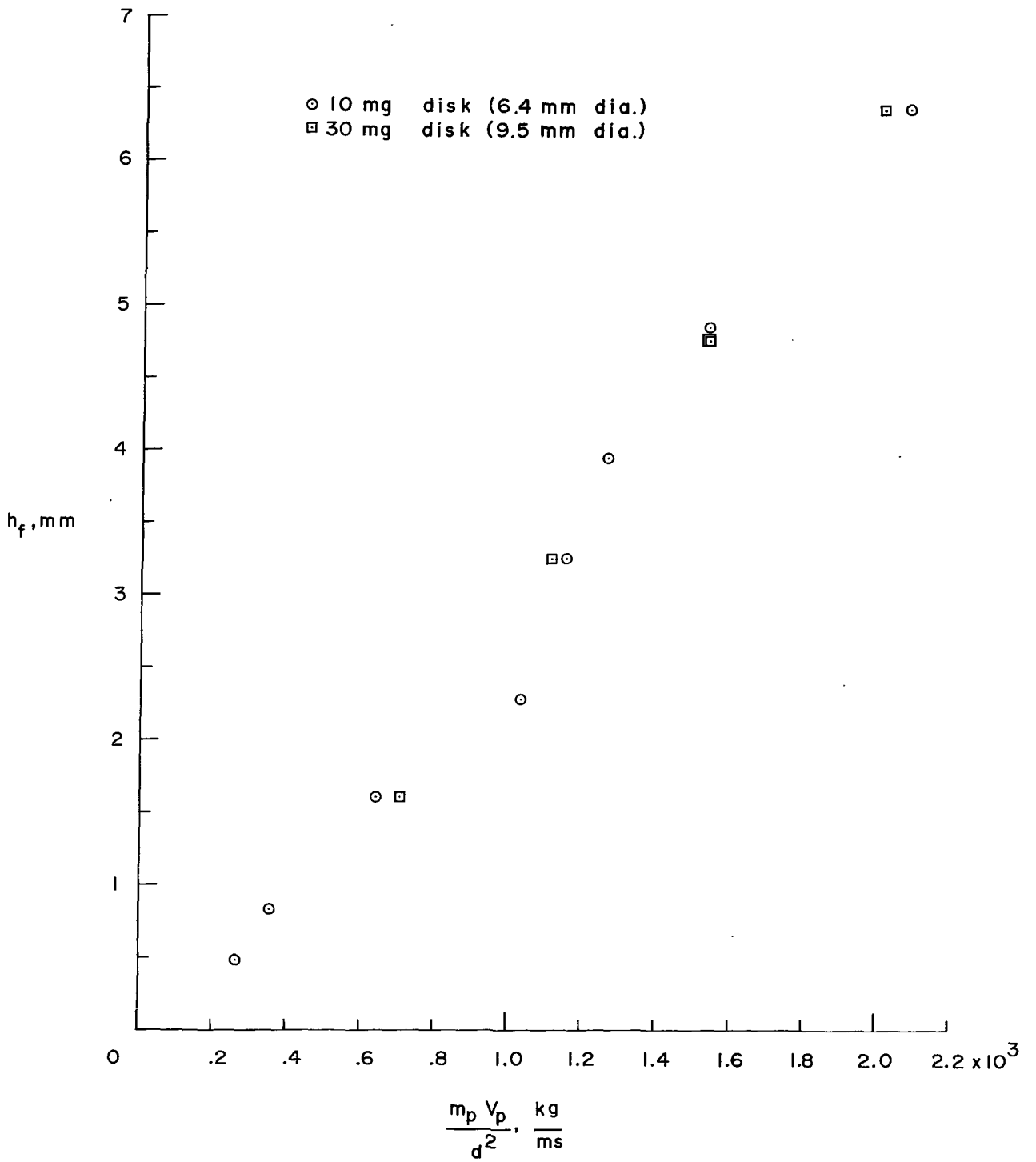

Figure 4.- Experimental variation of plate failure thickness with projectile momentum per unit area. Targets, 2024-T3 aluminum. Data obtained from reference 4.

NASA-Langley, 1969 —— 32 L-6429

NATIONAL AERONAUTICS AND SPACE ADMINISTRATION
WASHINGTON, D. C. 20546

OFFICIAL BUSINESS

FIRST CLASS MAIL

POSTAGE AND FEES PAID
NATIONAL AERONAUTICS AND
SPACE ADMINISTRATION

POSTMASTER: If Undeliverable (Section 158 Postal Manual) Do Not Return

"The aeronautical and space activities of the United States shall be conducted so as to contribute . . . to the expansion of human knowledge of phenomena in the atmosphere and space. The Administration shall provide for the widest practicable and appropriate dissemination of information concerning its activities and the results thereof."

—NATIONAL AERONAUTICS AND SPACE ACT OF 1958

NASA SCIENTIFIC AND TECHNICAL PUBLICATIONS

TECHNICAL REPORTS: Scientific and technical information considered important, complete, and a lasting contribution to existing knowledge.

TECHNICAL NOTES: Information less broad in scope but nevertheless of importance as a contribution to existing knowledge.

TECHNICAL MEMORANDUMS: Information receiving limited distribution because of preliminary data, security classification, or other reasons.

CONTRACTOR REPORTS: Scientific and technical information generated under a NASA contract or grant and considered an important contribution to existing knowledge.

TECHNICAL TRANSLATIONS: Information published in a foreign language considered to merit NASA distribution in English.

SPECIAL PUBLICATIONS: Information derived from or of value to NASA activities. Publications include conference proceedings, monographs, data compilations, handbooks, sourcebooks, and special bibliographies.

TECHNOLOGY UTILIZATION PUBLICATIONS: Information on technology used by NASA that may be of particular interest in commercial and other non-aerospace applications. Publications include Tech Briefs, Technology Utilization Reports and Notes, and Technology Surveys.

Details on the availability of these publications may be obtained from:

SCIENTIFIC AND TECHNICAL INFORMATION DIVISION

NATIONAL AERONAUTICS AND SPACE ADMINISTRATION

Washington, D.C. 20546